6.1. Introduction

The metal ions with ordered and disordered transition in perovskites are widely investigated. The hexagonal perovskites stabilized via doping of iron at the Ti-site with the doping amount of 0.06 - 0.84 [Akimoto *et al*. (1994), Megaw (1946), Vanderah *et al*. (1996)]. The two Fe^{3+} ion create one oxygen vacancy in the perovskite system. The lattice parameters of the doped perovskites increase with oxygen vacancy as well as doping amounts of iron at the site of titanium due to different ionic radius of cations [Shannon (1976)]. The magnetic materials attracted attention of researcher due to application of these materials in high density energy storage, electro-optic devices, microwave devices, magneto-optic recording, magnetic resonating imaging and drug delivery systems [Cullity and Graham (2011), McCurrie (1994), Sugimoto (1999), Kleemann and Binek (2013), Fujimori *et al*. (1971)]. The deficiencies at room temperature of multiferroics due to the chemical dissimilarities between magnetism and ferroelectricity, insulating ferromagnetic materials were developed via weak magnetoelectric coupling and low magnetic critical temperature [Eerenstein *et al*. (2006), Ma *et al*. (2011), Pradhan *et al*. (2013a), Pradhan *et al*. (2013b), Sharma *et al*. (2016), Sharma *et al*. (2015)]. The iron doping at titanium site was much favorable due to similar ionic radii [Rajamani *et al*. (2005), Maier and Cohn (2002), Maier *et al*. (2001)]. With the amount of iron dopant in hexagonal perovskites $BaTiO_{3-\delta}$ the ferromagnetic signal decreases at the room temperature [Lin *et al*. (2008a)]. The magnetic moment depends upon the various factors like temperatures, atmosphere [Wei *et al*. (2012), Lin *et al*. (2008b)] and sintering duration of the material [Lin and Shi (2012)]. The oxygen vacancies in iron substituted at titanium site ceramic materials, were maintained by mismatching of charge difference between Fe^{3+} and Ti^{4+} [Wei *et al*. (2011)]. The magnetic behavior of iron doped $Ba_4Y_2Ti_4O_{17}$ (BYTO) has not been explored yet with variation of temperatures. In this chapter $Ba_6Y_2Ti_{4-x}Fe_xO_{17}$ (x= 0.05, 0.1, 0.2) ceramics

termed as BYTFO-05, BTFO-1 and BYTFO-2 and all three compositions are also represented by BYTFO, synthesized by semi wet route and its temperature and frequency dependent electrical and magnetic properties were studied.

6.2. Experimental

$Ba_6Y_2Ti_{4-x}Fe_xO_{17}$ (x= 0.05, 0.1, 0.2) BYTFO-05, BYTFO-1 and BYTFO-2 ceramics were prepared by semi wet route in which standard aqueous solutions of barium, yttrium, and iron nitrate were used whereas Ti is added in the form of TiO_2 solid powder. All the analytical grade chemicals of $Ba(NO)_3.6H_2O$ (99 % Merck India), $Y(NO)_3.6H_2O$ (99.8 % Merck India), TiO_2 (99 % Sigma-Aldrich India), and $Fe(NO)_3.H_2O$ (98 % Merck India) were used in the above synthesis. Firstly, the stoichiometric amount of metal nitrates of barium, yttrium and iron were dissolved in double distilled water in separate beakers after that these three solutions were mixed in one beaker and then calculated amount of solid TiO_2 was added in this reaction mixture. Secondly, the equivalent amount of glycine to metal ions was also added and then heated on hot plate with constant stirring using magnetic stirrer at 70 - 80 ^{0}C. After evaporation of water a fluffy mass was obtained on combustion with sooty flame. This resultant powder was grounded with the help of agate and mortar to make it fine powder and calcined at 500 ^{0}C for 5 h and then 800 ^{0}C for 8 h. Further these calcined powders were used to make cylindrical pellets on applying 5 ton of pressure with the help of hydraulic press using polyvinyl alcohol as a binder. Finally, these pellets were sintered in muffle furnace at 1100 ^{0}C for 12 h. Powder diffraction patters was recorded by Rigaku miniflex 600 (Japan) with diffraction angle of 20 - 80^0 at scan rate of 1° per min keeping step size 0.02. Bright field TEM images and SAED patterns of synthesized materials recorded by HR TEM (TECHNAI G^2 TWIN), surface morphology and grain size and grain boundary were collected with the help of HR-SEM and elemental

mapping (FEI NOVA NANO SEM 450), DC Magnetic properties of materials such as M-T and M-H at few selected temperature were performed by MPMS (SQUID Magnetometer Quantum design), Dielectric properties such as capacitance, dielectric loss, impedance and resistance were measured by PSM1735 NumetriQ (Newton 4th Ltd U.K), temperature dependent ferroelectric properties measured by PE loop tracer (Marine India).

6.3. Results and discussion

6.3.1. Material Characterization

Figure 6.1 shows the X-ray diffraction patterns of BYTFO-05, BYTFO-1 and BYTFO-2 ceramics shows the single phase formation of all the materials sintered at 1100 ^{0}C. All peaks were index with the JCPDS file no 43-0417. The crystallite size was calculated with the help of Debye Scherer formula using three most intense peak.

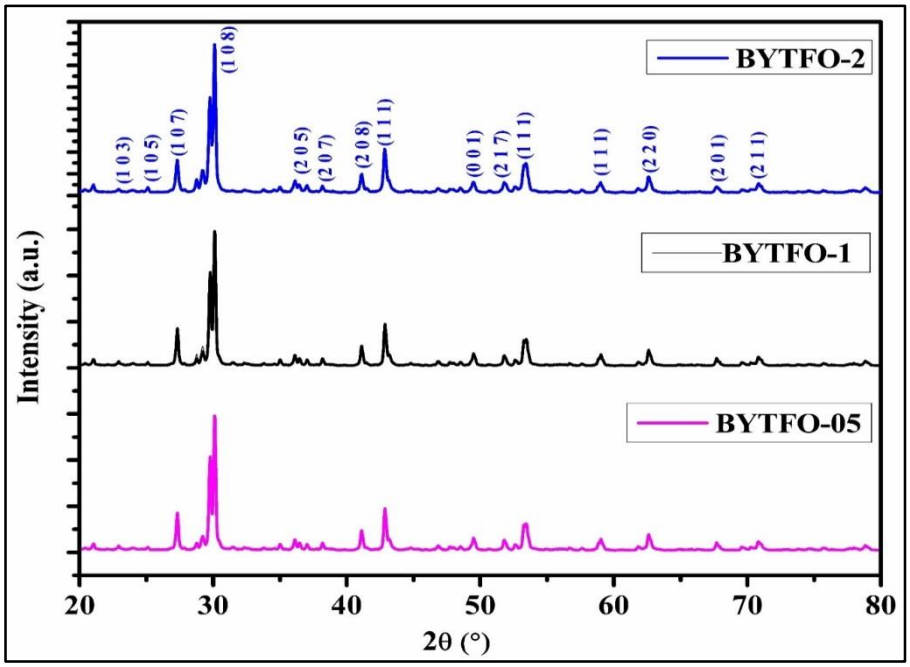

Figure 6.1 Powder XRD of BYTFO-05, BYTFO-1 and BYTFO-2 sintered at 1100 ^{0}C

The calculated average crystallite size in all three compounds is 35 ± 5 nm. The lattice parameters were calculated with the help of cell software and found to be a = b = 5.9260 Å, 5.9130 Å, 5.9107 Å and c = 29.5205 Å, 29.518 Å, 29.420 Å for BYTFO-05, BYTFO-1 and BYTFO-2 ceramics, respectively. To understand this decrease in lattice parameters, we compared parent hexagonal perovskite oxide $Ba_6Y_2Ti_4O_{17}$ in which the ionic radii of Ti^{4+} is 0.605 Å. The doping of Fe in this compound may be due to the presence of Fe^{3+} (0.645 Å) and Fe^{4+} (0.585 Å). The ratio of Fe^{3+}/Fe^{4+} causes the variation of lattice parameters. On increase of Fe amount this ratio also increase, and more Fe^{3+} substitute Ti^{4+} that leads to gradual decrease of both the lattice parameters a and c [Wei *et al*. (2010), Grey *et al*. (1998)]. Figure 6.2 (a, b and c) represents the TEM images of BYTFO-05, BYTFO-1 and BYTFO-2 respectively. These figures clearly indicate the presence of hexagonal shape particles in the BYTFO ceramic sintered at 1100 ^{0}C for 12 h. The average particle sizes of BYTFO-05, BYTFO-1 and BYTFO-2 are 160 nm, 133 nm and 100 nm respectively.

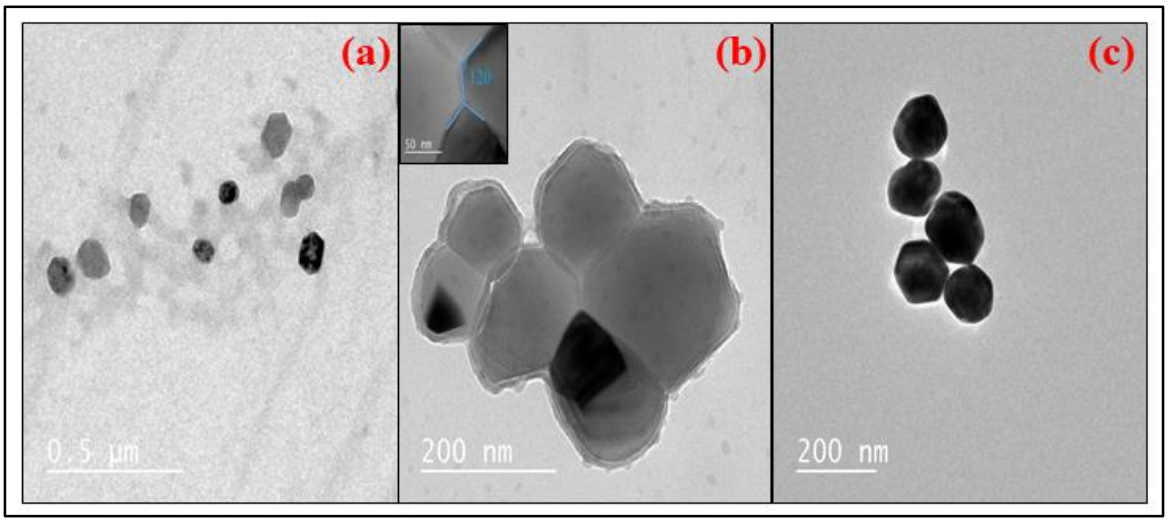

Figure 6.2 TEM images of BYTFO-05, BYTFO-1 and BYTFO-2 are shown in **(a)**, **(b)** and **(c)** respectively

In the inset of Figure 6.2 (b) a line drawn over the edge of hexagonal grains, the measured bond angle was found to be 120^0 which supports the hexagonal nature of synthesized materials. Figure 6.3 (a, b and c) shows homogeneous distribution of grains over a selected area of samples BYTFO-05, BYTFO-1 and BYTFO-2 respectively. There are some triangular, spherical and hexagonal grains distributed homogeneously in the material.

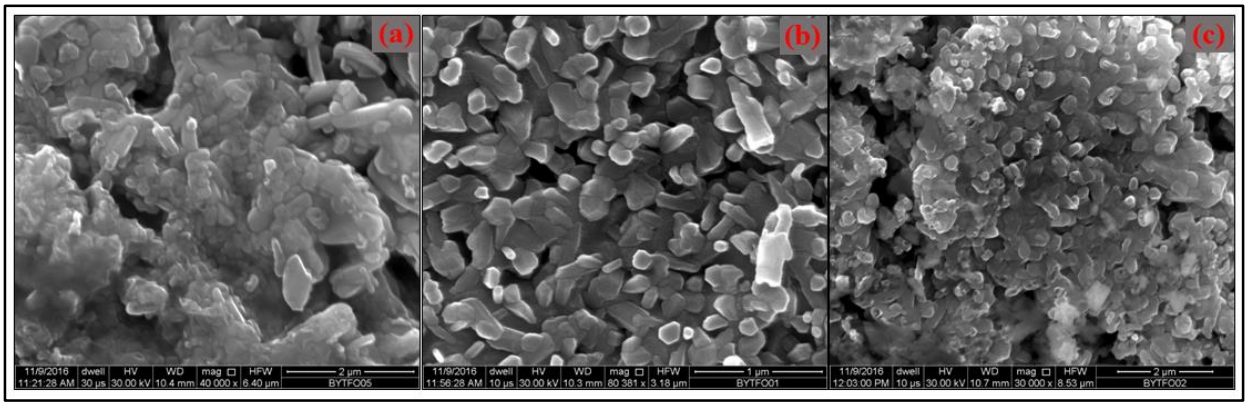

Figure 6.3 SEM images of BYTFO-05, BYTFO-1 and BYTFO-2 are shown in **(a)**, **(b)** and **(c)** respectively

Figure 6.4 represents elemental mapping of BYTFO-1 this indicates that each element of this material is homogeneously distributed. The elements are represented with color bars as atomic percentages and are shown in Figure 6.4 (f). The observed atomic percentage supports the molecular formulae of $Ba_4Y_2Ti_{3.9}Fe_{0.1}O_{17}$ (BYTFO-1) ceramic.

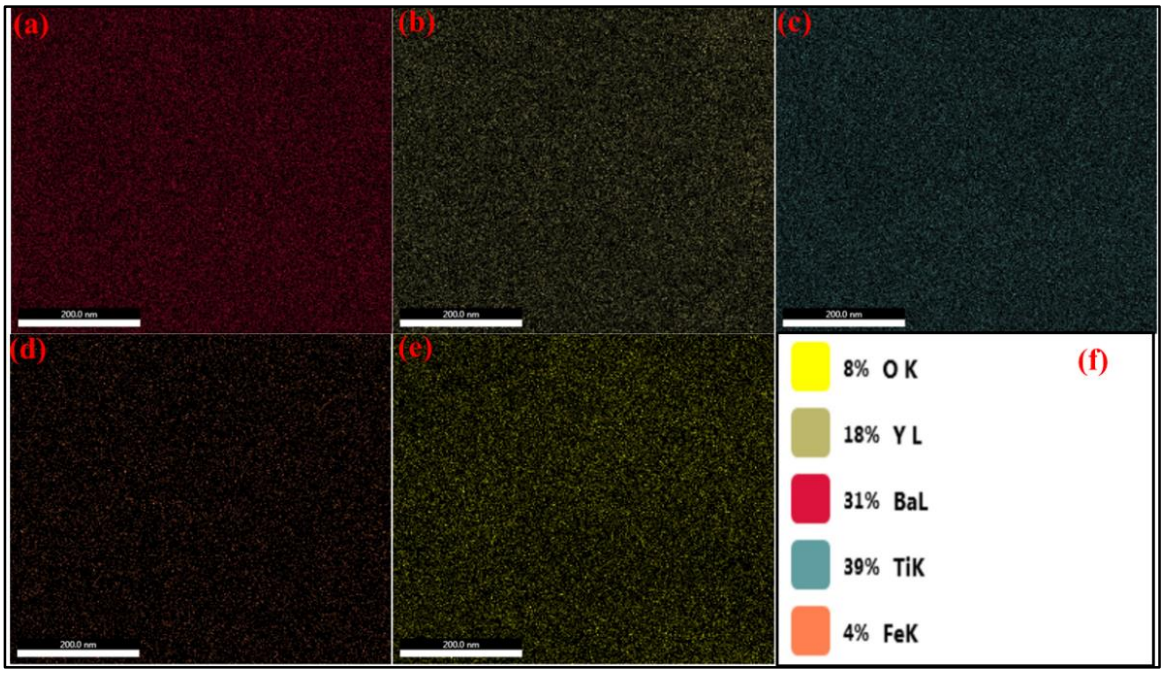

Figure 6.4 Elemental mapping and atomic percentages of BYTFO-1

6.3.2. Dielectric properties

Figure 6.5 shows the variation of dielectric constant of BYTFO-05, BYTFO-1 and BYTFO-2 as a function of frequency (10^2 to 10^6). The observed dielectric constants at 100 Hz of frequency were found to be 1.48 $\times 10^3$, 1.35 $\times 10^3$ and 9.19 $\times$ 10^2 for BYTFO-05, BYTFO-1 and BYTFO-2 respectively. The observed dielectric constant is smaller than that of undoped BYTO (Chapter 5). On increasing the amount of iron the dielectric constant decreases may be due to suppression of Ba/Ti disorder and absence of barrier layer formation at the grain boundary [Rai *et al*. (2011), Mu *et al*. (2010)]. The dielectric constant decreases very rapidly in the frequency range of 100 Hz to 1 kHz after that it remains constant up to 5 MHz.

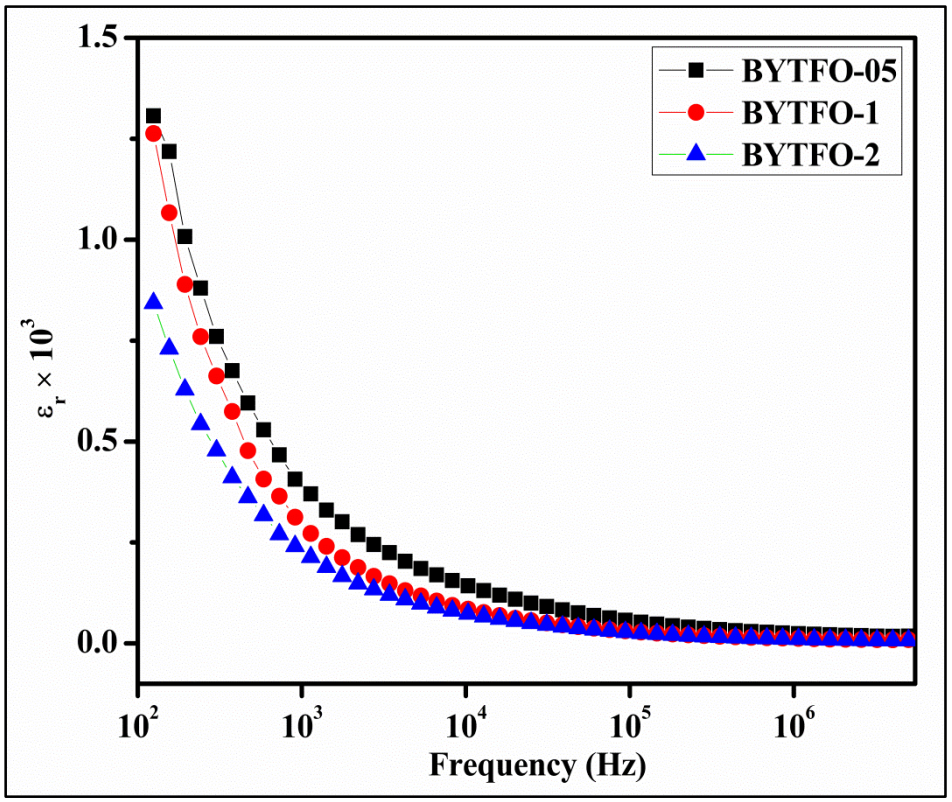

Figure 6.5 Dielectric constant *versus* frequency of BYTFO-05, BYTFO-1 and BYTFO-2 ceramics sintered at 1100 ^{0}C for 12 h

The high dielectric constant at low frequency simply comes from the fact that polarization of mixed dipoles in undoped BYTO (x = 0.0) ceramic, occurs simultaneously with the application of electric field [Hutagalung *et al*. (2009)]. As frequency increased, the heavy dipoles cannot follow the alternation of the applied field and only lighter dipoles respond to high frequency leading to drop in dielectric constant [Ni *et al*. (2006), Li *et al*. (2005)]. Addition of iron to BYTO ceramic caused the dielectric constant to decrease at low frequency as compared to pure BYTO ceramic. So it can be suggested that doping of iron resulted in lowering the concentration of heavy dipole and hence dielectric constant decreased with iron amount.

Figure 6.6 shows variation of the dielectric loss with frequency for BYTFO-05, BYTFO-1 and BYTFO-2 ceramics. The continuous decrease of tangent loss was observed with increasing frequency may be due to energy dissipation during polarization. The observed dielectric losses are 1.7, 1.6 and 1.1 for BYTFO-05, BYTFO-1 and BYTFO-2 respectively. The iron doped BYTO have higher dielectric loss as compared to undoped BYTO (Chapter 5) ceramic may be due to iron enhance conductivity of materials.

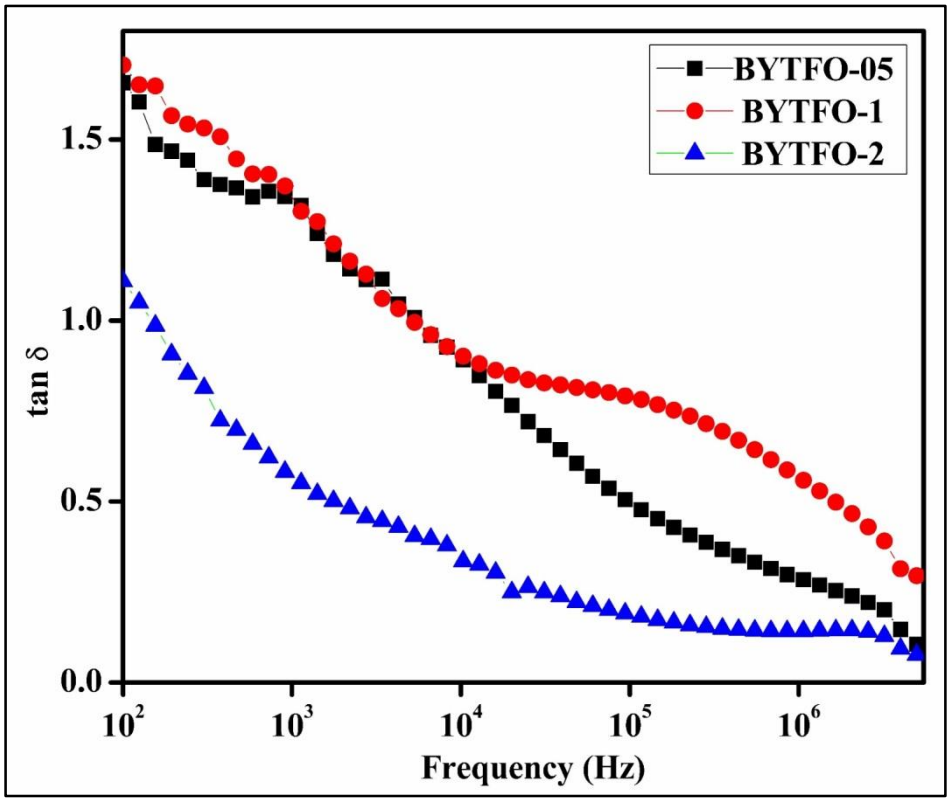

Figure 6.6 Variation of dielectric loss with frequency of BYTFO-05, BYTFO-1 and BYTFO-2 ceramics

Figure 6.7 (a, b and c) shows variation of dielectric constant with temperature for BYTFO-05, BYTFO-1 and BYTFO-2 respectively at 1 kHz frequency. Debye type relaxation was observed in all the samples (BYTFO-05, BYTFO-1 and BYTFO-2) it may be due to surface layer interfacial polarization [Zheng *et al*. (2016)]. For BYTFO-05 a gradual decrease of

dielectric constant from 300 to 400 K whereas for BYTFO-2 increases from 450 to 500 K. For BYTFO-1 a sharp dielectric constant peak is observed at 350 K.

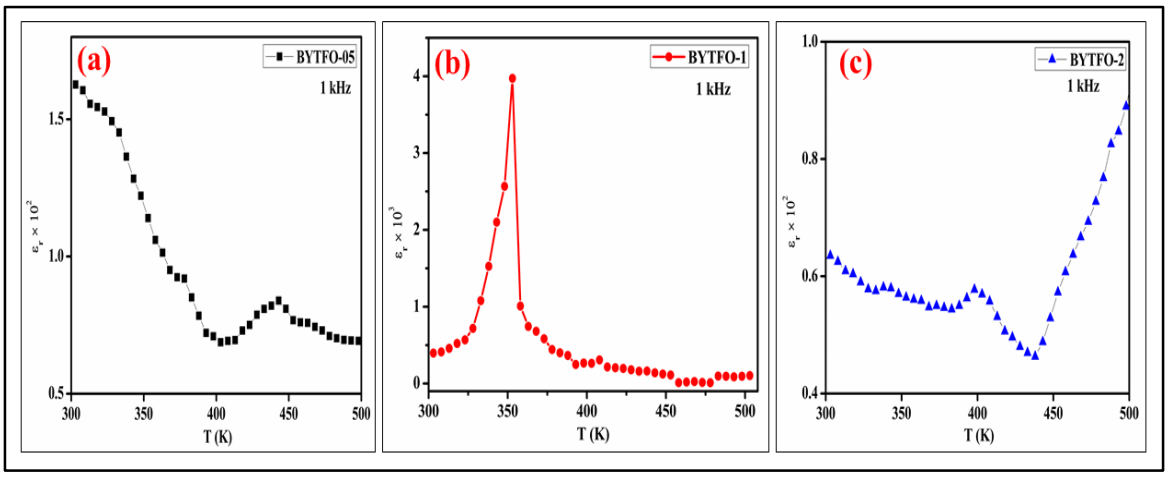

Figure 6.7 Variation of dielectric constant with temperature at 1 kHz for **(a)** BYTFO-05 **(b)** BYTFO-1 **(c)** BYTFO-2 ceramics sintered at 1100 ^{0}C for 12 h

Figure 6.8 shows the temperature dependence of dielectric loss (tan δ) at 1 kHz frequency of BYTFO-05, BYTFO-1 and BYTFO-2 ceramics. For thermally activated relaxation a sharp peak was observed in BYTFO-1 which broadens in case of BYTFO-05 and BYTFO-2. Temperature dependent dielectric loss behavior indicates the ferroelectric nature of ceramic [Singh *et al*. (2013)]. This dielectric dispersion is related to a conductivity phenomenon, obeying the Arrhenius-type thermal activation law [Singh *et al*. (2015)].

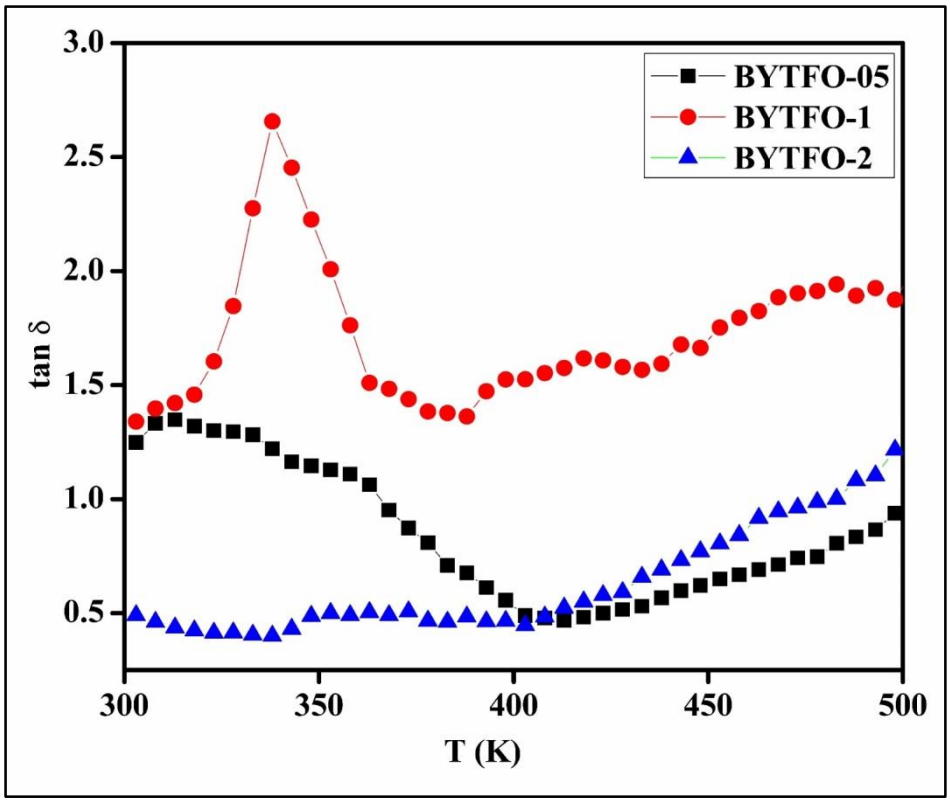

Figure 6.8 Variation of dielectric loss with temperature at 1 kHz for BYTFO-05, BYTFO-1 and BYTFO-2 ceramics

The complex impedance plane plot (Z' vs Z") of iron doped BYTO ceramics at 300 K was shown in Figure 6.9. The Complex plane impedance is the powerful technique which separates the contribution of the grains, and grain boundaries, and electrode specimen interface to the total resistance and capacitance. It is observed from the Figure 6.9 that the experimental impedance data only cover a part of semicircular arcs, due to limit of measurement frequency range of the instrument. Only a fraction of grain boundary arc is observed in all ceramics. The doping of iron affects the value of grains and grain boundary resistance. A large decrease of resistance of grain boundary with iron amount represents charge compensation between iron and Ti at the grain boundary.

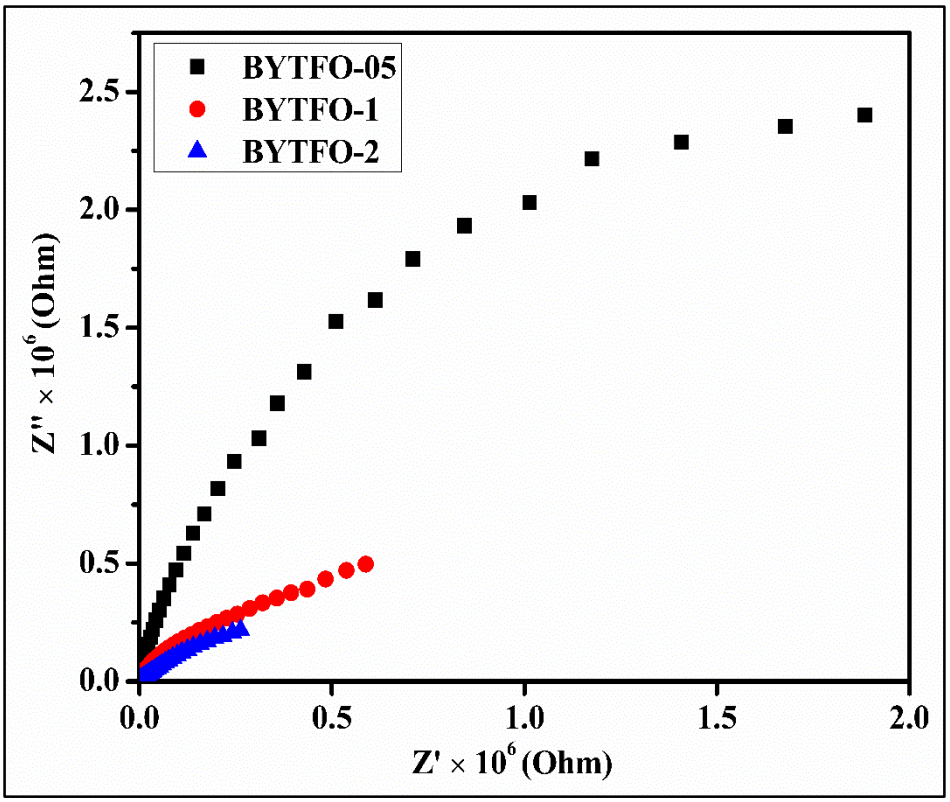

Figure 6.9 Impedance plane plot (Z' vs Z") of BYTFO-05, BYTFO-1 and BYTFO-2 ceramics at 300 K

6.3.3. Magnetic properties

The M-H hysteresis loop of BYTFO-05 shown in Figure 6.10 indicates ferromagnetic nature of the material. The clear vision of remanent magnetization and coercive field was shown in the inset of Figure 6.10. The observed remanent magnetization and saturation magnetization listed in table 6.1 which decreases with temperature for all the three samples due to disordering of magnetic domains. The coercive field decreases with increasing temperature indicates material becomes soft magnets at higher temperature. The magnetic hysteresis of BYTFO-1 and BYTFO-2 is shown in Figure 6.11 and 6.12 respectively.

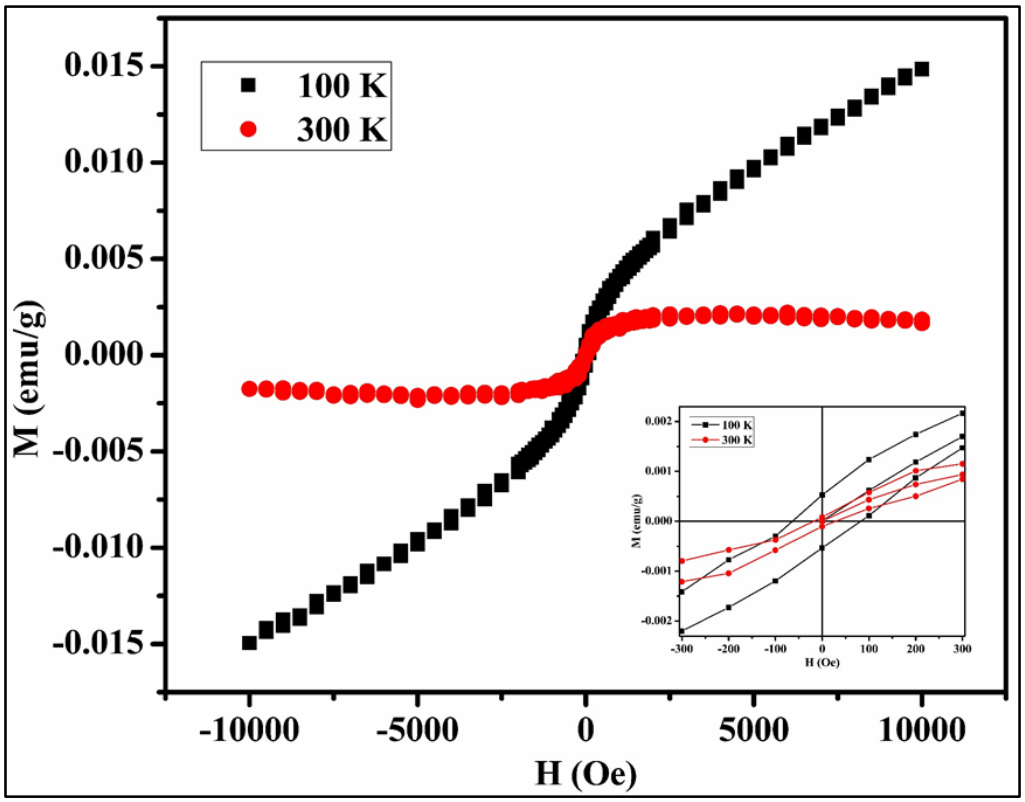

Figure 6.10 M-H hysteresis loop of BYTFO-05 at 100 and 300 K

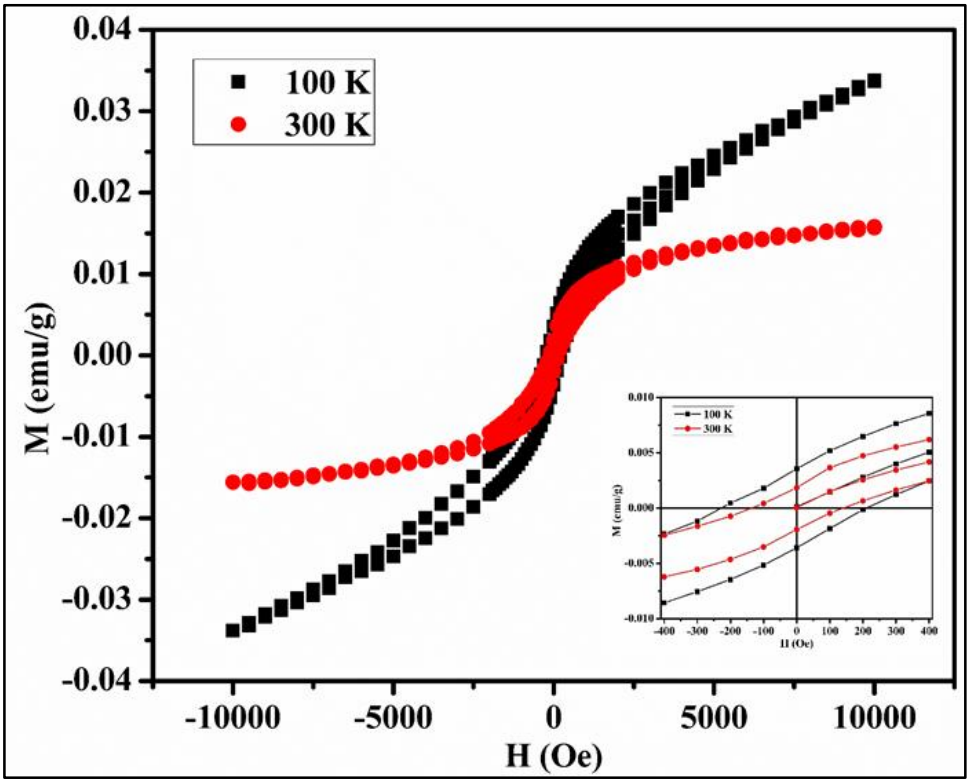

Figure 6.11 M-H hysteresis loop of BYTFO-1

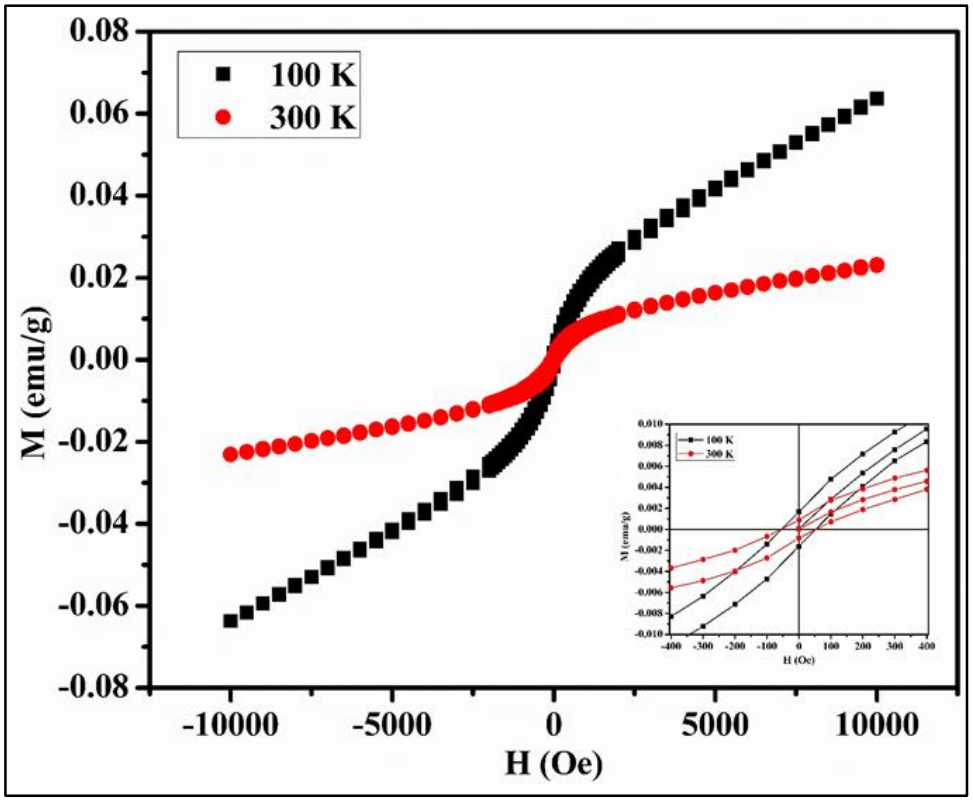

Figure 6.12 M-H loop of BYTFO-2

Table 6.1. Remanent magnetization, saturation magnetization and magnetic coercivity of $Ba_6Y_2Ti_{4-x}Fe_xO_{17}$ (x= 0.05, 0.1 and 0.2) materials

Temperature (K)	BYTFO-05			BYTFO-1			BYTFO-2		
	Mr (emu/g) $x10^{-4}$	Ms (emu/g) $x10^{-3}$	Ec (Oe)	Mr (emu/g) $\times 10^{-3}$	Ms (emu/g) $\times 10^{-2}$	Ec (Oe)	Mr (emu/g) $\times 10^{-3}$	Ms (emu/g) $\times 10^{-2}$	Ec (Oe)
100	5.277	6.0	80.66	3.56	1.72	199.88	1.67	2.27	49.19
300	0.825	2.17	26.07	0.853	1.21	142.85	0.889	1.16	49.19

Both sample shows ferromagnetic character of material having inverse behavior of remanent magnetization with temperature. From the Table 6.1 saturation magnetization increase with increasing amount of iron whereas coercivity of BYTFO-1 is very high may be due to inhomogeneous distribution of grains. The coercivity of BYTFO-05 and BYTFO-1 is temperature dependent and soft magnetic character increase with temperature whereas BYTFO-2 coercivity is independent on temperature.

6.3.4. Ferroelectric properties

The room temperature ferroelectric properties of Fe-doped $Ba_4Y_2Ti_4O_{17}$ (BYTO) ceramic were shown in Figure 6.13. Ferroelectricity in these materials was due to off center shift of transition metal ions (Ti). The transition metal ion Ti^{4+} binds covalently with oxygen with its empty d orbital [Khomskii (2009)]. Ferroelectricity of material is decreased on increasing iron concentration is understandable because hexagonal phase formation promotes by iron doping at titanium site. On increasing iron concentration shifting of Ti atom increase that reduces the Fe-Ti bond length due to 3d orbital overlapping. This overlapping is more effective at the top compare to bottom interface [Pan *et al*. (2011)]. The valence state of iron reduced due to electron traps of oxygen vacancies and these oxygen vacancies reduces ferroelectricity [Griffin *et al*. (2005)].

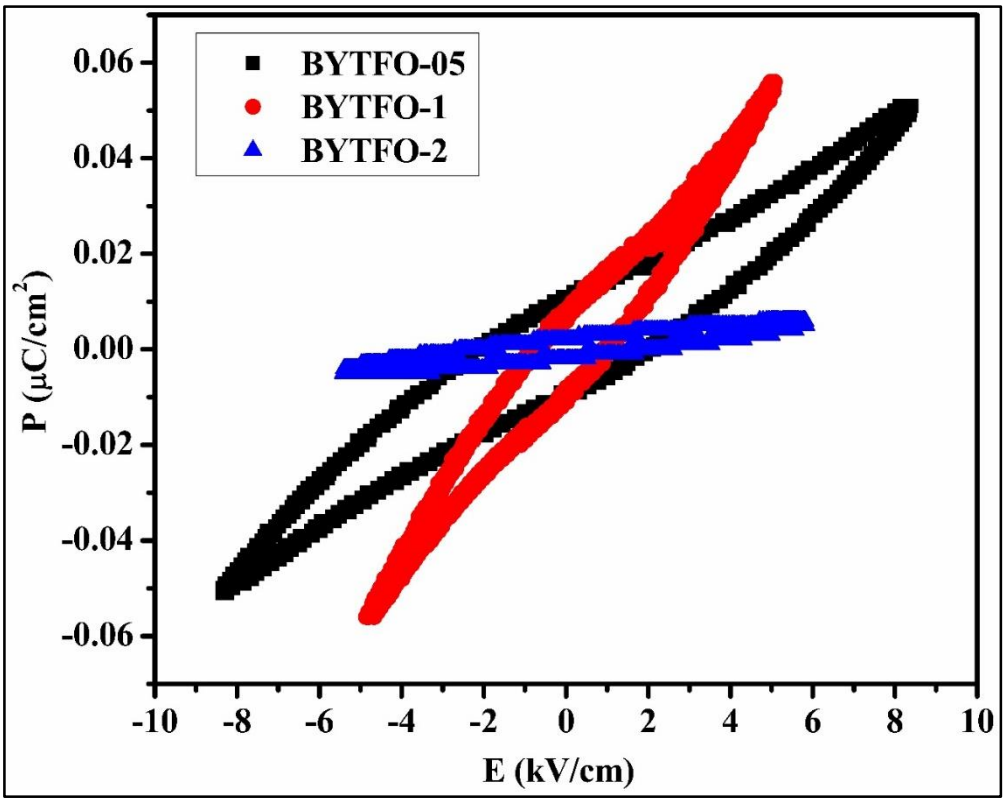

Figure 6.13 PE hysteresis loop of BYTFO-05, BYTFO-1 and BYTFO-2 ceramics

6.4. Conclusion

Single phase formation of all the three samples BYTFO-05, BYTFO-1 and BYTFO-2 indicates the doping of iron at the site of titanium up to the extent of 0.2. The images having bond angle 120° observed from transmission electron microscopy confirms hexagonal perovskite nature of material. Purity and presence of corresponding elements in material were explored by HR SEM EDX and elemental mapping. On increasing the amount of iron in BYTO ceramic the dielectric constant decreases which may be due to suppression of Ba/Ti disorder and absence of barrier layer formation at the grain boundary. Ferroelectricity of the ceramic decreases on increasing iron concentration is clearly understood because hexagonal phase formation promotes by iron at titanium site.